Bull Earthquake Eng (2011) 9:603–621
DOI 10.1007/s10518-010-9214-6

ORIGINAL RESEARCH PAPER

# Estimation of the seismic energy demands of two-way asymmetric-plan building systems

**Jui-Liang Lin · Keh-Chyuan Tsai**

Received: 23 June 2009 / Accepted: 26 September 2010 / Published online: 12 October 2010


**Abstract** This paper proposes a method for the estimation of the seismic energy demands of two-way asymmetric-plan buildings under bi-directional ground excitations. The modal absorbed energies of asymmetric-plan buildings are estimated by using the three-degree-of-freedom (3DOF) modal systems. The 3DOF modal system represents the two roof translations versus the two base shears and the roof rotation versus the base torque relationships of each vibration mode of two-way asymmetric-plan buildings. Not only the total absorbed energy but also the portions of the total absorbed energy contributed from translational and rotational deformations can be respectively estimated. This study verifies the relationship between the signs of modal eccentricities and the trend of uneven distribution of modal absorbed energy on floor-plan edges of asymmetric-plan buildings. The accuracy of the proposed method was verified by analyzing one 3-storey and one 20-storey two-way asymmetric-plan buildings subjected to bi-directional ground motions. The computational efficiency of the proposed method is confirmed by comparing the computation time with that required by using the nonlinear response history analysis.

**Keywords** Asymmetric-plan buildings · Modal response history analysis · Modal system · Absorbed energy · Torsion · Eccentricity · Seismic behavior

## 1 Introduction

It is well known that the structural damages not only related to the maximum responses but also the inelastic excursion occurred below the maximum responses. Thus, in addition to the ductility demand, energy demand also plays a key role for assessing the seismic damages of structures (Housner 1956; Park and Ang 1985). The input seismic energy, $E_i$, is equal to the

J.-L. Lin
National Center for Research on Earthquake Engineering, Taipei, Taiwan, ROC
e-mail: jllin@ncree.org.tw

K.-C. Tsai (✉)
Department of Civil Engineering, National Taiwan University, Taipei, Taiwan, ROC
e-mail: kctsai@ncree.org.tw

summation of the kinetic energy, $E_k$, viscous damping energy, $E_\xi$, and absorbed energy, $E_a$. Absorbed energy $E_a$ consists of the recoverable elastic strain energy, $E_s$, and the irrecoverable hysteretic energy, $E_h$. Chou (2001) indicated that $E_a$ is very close to $E_h$ when the ductility factor is larger than two. In order to understand the variation of energy demand for various structures, energy spectra were constructed by using SDOF systems (Fajfar et al. 1989). For structural responses with significant higher mode effects, it is evident that considering single modal absorbed energy is not enough. Although the "vibration modes" are changed from time to time for inelastic structures, Chou and Uang (2003) proposed a method for estimating the first and the second "modal" absorbed energies of symmetric-plan multi-storey buildings. Furthermore, by using the concepts of modal pushover analysis (Chopra and Goel 2002), the hysteretic energies of the first few vibration "modes" of symmetric-plan multi-storey buildings were computed and summed together as the estimated total hysteretic energy of the buildings (Prasanth et al. 2008). Considering the complicated behaviors of asymmetric-plan buildings under bi-directional ground excitations, Prasanth et al. (2008) concluded that the estimation of seismic energy demands of asymmetric-plan buildings is an issue worthy of future research. To the best of the authors' knowledge, except the computation-intensive and time-consuming nonlinear response history analysis (RHA) method, it seems still no efficient approach for the estimation of absorbed energies of asymmetric-plan buildings.

Furthermore, the unevenly plan-wise distribution of the hysteretic energy demands on stiff sides (SS) and flexible sides (FS) of asymmetric-plan buildings were diversely concluded by different researchers (Goel 1997). Some researchers pointed out that the elements on the SS of code-designed asymmetric-plan systems are likely to suffer more damage, whereas the elements on the FS are expected to suffer less or similar damage compared to those in the corresponding symmetric system. On the contrary, Goel (1997) concluded that the elements on the FS could undergo much larger hysteretic energy demands in an asymmetric-plan system than those in the corresponding symmetric systems. The elements on the SS, on the other hand, might not necessarily experience any larger hysteretic energy demands in asymmetric-plan systems. Hence, it indicates that the reasonable explanations for the phenomenon of different energy demands on floor-plan edges of asymmetric-plan buildings are still not clear.

Due to the non-proportionality between the modal translation and the modal rotation of inelastic asymmetric-plan buildings, the three-degree-of-freedom (3DOF) modal systems have been developed and applied to the modal response history analyses of two-way asymmetric-plan buildings (Lin and Tsai 2008). Each 3DOF modal system simultaneously represents the two roof translations vs. the two base shears and the roof rotation versus the base torque relationships obtained from the modal pushover analysis of an asymmetric-plan building. In this study, the modal absorbed energies of asymmetric-plan buildings are computed by using the 3DOF modal systems instead of the conventional single-degree-of-freedom (SDOF) modal systems. In addition, the relationships between the modal eccentricities and the unevenly plan-wise distribution of absorbed energy of asymmetric-plan buildings are investigated.

## 2 Theorectical background

### 2.1 Three-degree-of-freedom modal systems

For the sake of completeness and to make it easier to adopt the notations in the rest of this paper, we briefly present the results of the 3DOF modal systems herein. More details can be found in Lin and Tsai (2008).

In order to be consistent with the coordinate system used in the previous study (Lin and Tsai 2008), the two plan axes are the X- and Z-axis. The Y-axis is upward (opposite to the direction of gravity). The proportionally damped two-way asymmetric-plan buildings with each floor simulated as a rigid diaphragm are considered in this research. The equation of motion for an $N$-storey two-way asymmetric-plan building subjected to bi-directional ground excitations is

$$\begin{aligned}\mathbf{M}\ddot{\mathbf{u}}+\mathbf{C}\dot{\mathbf{u}}+\mathbf{K}\mathbf{u}&=-\mathbf{M}\boldsymbol{\iota}_x\ddot{u}_{gx}(t)-\mathbf{M}\boldsymbol{\iota}_z\ddot{u}_{gz}(t)\\&=-\sum_{n=1}^{3N}\mathbf{s}_{xn}\ddot{u}_{gx}(t)-\sum_{n=1}^{3N}\mathbf{s}_{zn}\ddot{u}_{gz}(t)=-\sum_{n=1}^{3N}\Gamma_{xn}\mathbf{M}\boldsymbol{\varphi}_n\ddot{u}_{gx}(t)-\sum_{n=1}^{3N}\Gamma_{zn}\mathbf{M}\boldsymbol{\varphi}_n\ddot{u}_{gz}(t)\\&=-\sum_{n=1}^{3N}\left(\Gamma_{xn}\ddot{u}_{gx}+\Gamma_{zn}\ddot{u}_{gz}\right)\mathbf{M}\boldsymbol{\varphi}_n,\end{aligned}\tag{1}$$

in which the displacement vector, $\mathbf{u}$, mode shape, $\boldsymbol{\varphi}_n$, mass matrix, $\mathbf{M}$, stiffness matrix, $\mathbf{K}$, influence vectors, $\boldsymbol{\iota}_x, \boldsymbol{\iota}_z$, modal inertia force distributions, $\mathbf{s}_{xn}, \mathbf{s}_{zn}$, and modal participation factors, $\Gamma_{xn}, \Gamma_{zn}$, are

$$\mathbf{u}=\begin{bmatrix}\mathbf{u}_x\\\mathbf{u}_z\\\mathbf{u}_\theta\end{bmatrix}_{3N\times1},\quad\boldsymbol{\varphi}_n=\begin{bmatrix}\boldsymbol{\varphi}_{xn}\\\boldsymbol{\varphi}_{zn}\\\boldsymbol{\varphi}_{\theta n}\end{bmatrix}_{3N\times1},\quad\mathbf{M}=\begin{bmatrix}\mathbf{m}_x&0&0\\0&\mathbf{m}_z&0\\0&0&\mathbf{I}_0\end{bmatrix}_{3N\times3N},\quad\mathbf{K}=\begin{bmatrix}\mathbf{k}_{xx}&\mathbf{k}_{xz}&\mathbf{k}_{x\theta}\\\mathbf{k}_{zx}&\mathbf{k}_{zz}&\mathbf{k}_{z\theta}\\\mathbf{k}_{\theta x}&\mathbf{k}_{\theta z}&\mathbf{k}_{\theta\theta}\end{bmatrix}_{3N\times3N}$$

$$\boldsymbol{\iota}_x=\begin{bmatrix}\mathbf{1}\\\mathbf{0}\\\mathbf{0}\end{bmatrix},\boldsymbol{\iota}_z=\begin{bmatrix}\mathbf{0}\\\mathbf{1}\\\mathbf{0}\end{bmatrix},\mathbf{s}_{xn}=\Gamma_{xn}\mathbf{M}\boldsymbol{\varphi}_n,\ \mathbf{s}_{zn}=\Gamma_{zn}\mathbf{M}\boldsymbol{\varphi}_n,\ \Gamma_{xn}=\frac{\boldsymbol{\varphi}_n^T\mathbf{M}\boldsymbol{\iota}_x}{\boldsymbol{\varphi}_n^T\mathbf{M}\boldsymbol{\varphi}_n},\ \Gamma_{zn}=\frac{\boldsymbol{\varphi}_n^T\mathbf{M}\boldsymbol{\iota}_z}{\boldsymbol{\varphi}_n^T\mathbf{M}\boldsymbol{\varphi}_n}\tag{2}$$

When only the force $-\left(\Gamma_{xn}\ddot{u}_{gx}+\Gamma_{zn}\ddot{u}_{gz}\right)\mathbf{M}\boldsymbol{\varphi}_n$ is applied to the building, the equation of motion (Eq. 1) becomes

$$\mathbf{M}\ddot{\mathbf{u}}_n+\mathbf{C}\dot{\mathbf{u}}_n+\mathbf{K}\mathbf{u}_n=-\left(\Gamma_{xn}\ddot{u}_{gx}+\Gamma_{zn}\ddot{u}_{gz}\right)\mathbf{M}\boldsymbol{\varphi}_n,\ n=1\sim3N,\tag{3}$$

in which $\mathbf{u}_n$ is the $n$-th modal displacement response and $\mathbf{u}=\sum_{n=1}^{3N}\mathbf{u}_n=\sum_{n=1}^{3N}\boldsymbol{\varphi}_nD_n$. $D_n$ is the generalized modal coordinate. By re-defining $\mathbf{u}_n$ equal to $\begin{bmatrix}\boldsymbol{\varphi}_{xn}&\mathbf{0}&\mathbf{0}\\\mathbf{0}&\boldsymbol{\varphi}_{zn}&\mathbf{0}\\\mathbf{0}&\mathbf{0}&\boldsymbol{\varphi}_{\theta n}\end{bmatrix}_{3N\times3}\begin{bmatrix}D_{xn}\\D_{zn}\\D_{\theta n}\end{bmatrix}_{3\times1}$, the 3DOF modal equation of motion for the $n$-th vibration mode is obtained as

$$\mathbf{M}_n\ddot{\mathbf{D}}_n+\mathbf{C}_n\dot{\mathbf{D}}_n+\mathbf{K}_n\mathbf{D}_n=-\left(\Gamma_{xn}\ddot{u}_{gx}+\Gamma_{zn}\ddot{u}_{gz}\right)\mathbf{M}_n\mathbf{1},\ n=1\sim3N\tag{4}$$

where

$$\mathbf{M}_n=\begin{bmatrix}\boldsymbol{\varphi}_{xn}^T\mathbf{m}_x\boldsymbol{\varphi}_{xn}&0&0\\0&\boldsymbol{\varphi}_{zn}^T\mathbf{m}_z\boldsymbol{\varphi}_{zn}&0\\0&0&\boldsymbol{\varphi}_{\theta n}^TI_0\boldsymbol{\varphi}_{\theta n}\end{bmatrix}_{3\times3},\ \mathbf{D}_n=\begin{bmatrix}D_{xn}\\D_{zn}\\D_{\theta n}\end{bmatrix}_{3\times1},\ \mathbf{1}=\begin{bmatrix}1\\1\\1\end{bmatrix}_{3\times1}$$

$$\mathbf{C}_n=\begin{bmatrix}\boldsymbol{\varphi}_{xn}^T\mathbf{c}_{xx}\boldsymbol{\varphi}_{xn}&\boldsymbol{\varphi}_{xn}^T\mathbf{c}_{xz}\boldsymbol{\varphi}_{zn}&\boldsymbol{\varphi}_{xn}^T\mathbf{c}_{x\theta}\boldsymbol{\varphi}_{\theta n}\\\boldsymbol{\varphi}_{zn}^T\mathbf{c}_{zx}\boldsymbol{\varphi}_{xn}&\boldsymbol{\varphi}_{zn}^T\mathbf{c}_{zz}\boldsymbol{\varphi}_{zn}&\boldsymbol{\varphi}_{zn}^T\mathbf{c}_{z\theta}\boldsymbol{\varphi}_{\theta n}\\\boldsymbol{\varphi}_{\theta n}^T\mathbf{c}_{\theta x}\boldsymbol{\varphi}_{xn}&\boldsymbol{\varphi}_{\theta n}^T\mathbf{c}_{\theta z}\boldsymbol{\varphi}_{zn}&\boldsymbol{\varphi}_{\theta n}^T\mathbf{c}_{\theta\theta}\boldsymbol{\varphi}_{\theta n}\end{bmatrix}_{3\times3},$$

$$\mathbf{K}_n=\begin{bmatrix}\boldsymbol{\varphi}_{xn}^T\mathbf{k}_{xx}\boldsymbol{\varphi}_{xn}&\boldsymbol{\varphi}_{xn}^T\mathbf{k}_{xz}\boldsymbol{\varphi}_{zn}&\boldsymbol{\varphi}_{xn}^T\mathbf{k}_{x\theta}\boldsymbol{\varphi}_{\theta n}\\\boldsymbol{\varphi}_{zn}^T\mathbf{k}_{zx}\boldsymbol{\varphi}_{xn}&\boldsymbol{\varphi}_{zn}^T\mathbf{k}_{zz}\boldsymbol{\varphi}_{zn}&\boldsymbol{\varphi}_{zn}^T\mathbf{k}_{z\theta}\boldsymbol{\varphi}_{\theta n}\\\boldsymbol{\varphi}_{\theta n}^T\mathbf{k}_{\theta x}\boldsymbol{\varphi}_{xn}&\boldsymbol{\varphi}_{\theta n}^T\mathbf{k}_{\theta z}\boldsymbol{\varphi}_{zn}&\boldsymbol{\varphi}_{\theta n}^T\mathbf{k}_{\theta\theta}\boldsymbol{\varphi}_{\theta n}\end{bmatrix}_{3\times3}\tag{5}$$

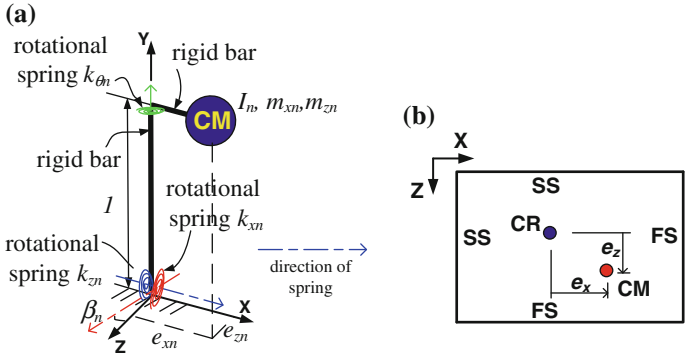


**Fig. 1** **a** The $n$-th 3DOF modal system. **b** The definitions of FS, SS and the sign conventions of eccentricities

$D_{xn}$, $D_{zn}$, and $D_{\theta n}$, are referred to as the X- and Z-directional modal translations and modal rotation respectively. The $n$-th 3DOF modal system corresponding to the 3DOF modal equation of motion is shown in Fig. 1a. The elastic properties of the $n$-th 3DOF modal system are as follows:

$$\beta_n = \tan^{-1}\left(\frac{\boldsymbol{\varphi}_{zn}^T \mathbf{k}_{zx} \boldsymbol{\varphi}_{xn}}{\boldsymbol{\varphi}_{xn}^T \mathbf{k}_{xx} \boldsymbol{\varphi}_{xn}}\right), \quad k_{xn} = \frac{\boldsymbol{\varphi}_{xn}^T \mathbf{k}_{xx} \boldsymbol{\varphi}_{xn}}{C^2}, \quad k_{zn} = \boldsymbol{\varphi}_{zn}^T \mathbf{k}_{zz} \boldsymbol{\varphi}_{zn} - k_{xn} S^2$$

$$\begin{bmatrix} e_{xn} \\ e_{zn} \end{bmatrix} = \begin{bmatrix} k_{xn} SC & -k_{xn} C^2 \\ k_{zn} + k_{xn} S^2 & -k_{xn} SC \end{bmatrix}^{-1} \begin{bmatrix} \boldsymbol{\varphi}_{xn}^T \mathbf{k}_{x\theta} \boldsymbol{\varphi}_{\theta n} \\ \boldsymbol{\varphi}_{zn}^T \mathbf{k}_{z\theta} \boldsymbol{\varphi}_{\theta n} \end{bmatrix},$$

$$k_{\theta n} = \boldsymbol{\varphi}_{\theta n}^T \mathbf{k}_{\theta\theta} \boldsymbol{\varphi}_{\theta n} - e_{xn}^2 k_{zn} - (e_{xn} S - e_{zn} C)^2 k_{xn}$$

$$m_{xn} = \boldsymbol{\varphi}_{xn}^T \mathbf{m}_x \boldsymbol{\varphi}_{xn}, \quad m_{zn} = \boldsymbol{\varphi}_{zn}^T \mathbf{m}_z \boldsymbol{\varphi}_{zn}, I_n = \boldsymbol{\varphi}_{\theta n}^T \mathbf{I}_0 \boldsymbol{\varphi}_{\theta n} \tag{6}$$

where $C = cos\beta_n$ and $S = sin\beta_n$. The inelastic parameters of the $n$-th 3DOF modal system, including the yielding moments $M_{yxn}$, $M_{yzn}$, $M_{y\theta n}$ and the post-yielding stiffness $k'_{xn}$, $k'_{zn}$, $k'_{\theta n}$ of the three rotational springs of the 3DOF modal system (Fig. 1a), are

$$M_{yxn} = A_{xny} m_{xn}, \quad M_{yzn} = A_{zny} m_{zn} \tag{7a}$$

$$M_{y\theta n} = A_{\theta ny} I_n + A_{xny} m_{xn} e_{zn} - A_{zny} m_{zn} e_{xn} \tag{7b}$$

$$k'_{xn} = \frac{m_{xn}}{\dfrac{m_{xn}}{k_{xn}} + \dfrac{(I_n + m_{xn} e_{zn} - m_{zn} e_{xn})\, e_{zn}}{k_{\theta n}} - \dfrac{(I_n + m_{xn} e_{zn} - m_{zn} e_{xn})\, e_{zn}}{k'_{\theta n}}} \tag{7c}$$

$$k'_{zn} = \frac{m_{zn}}{\dfrac{m_{zn}}{k_{zn}} - \dfrac{(I_n + m_{xn} e_{zn} - m_{zn} e_{xn})\, e_{xn}}{k_{\theta n}} + \dfrac{(I_n + m_{xn} e_{zn} - m_{zn} e_{xn})\, e_{xn}}{k'_{\theta n}}} \tag{7d}$$

$$k'_{\theta n} = k_{\theta n} \cdot \alpha_{\theta n} \tag{7e}$$

where $A_{xny}$, $A_{zny}$ and $A_{\theta ny}$ are the yielding accelerations and $\alpha_{xn}$, $\alpha_{zn}$ and $\alpha_{\theta n}$ are the post-yielding stiffness ratios of the three pushover curves idealized as three bilinear curves in the acceleration-displacement-response-spectra (ADRS) format. The stated three pushover curves, obtained from the modal pushover analysis of the original building, represent the

relationships of the two roof translations versus the two base shears and the roof rotation versus the base torque. The $n$-th modal response $\mathbf{D}_n$ is obtained by using the step-by-step integration of Eq. 4. The total displacement response $\mathbf{u}$ of the original building is obtained as

$$\mathbf{u} = \sum_{n=1}^{3N} \mathbf{u}_n = \sum_{n=1}^{3N} \mathbf{\Phi}_n \mathbf{D}_n = \sum_{n=1}^{3N} \begin{bmatrix} \boldsymbol{\varphi}_{xn} & \mathbf{0} & \mathbf{0} \\ \mathbf{0} & \boldsymbol{\varphi}_{zn} & \mathbf{0} \\ \mathbf{0} & \mathbf{0} & \boldsymbol{\varphi}_{\theta n} \end{bmatrix}_{3N\times 3} \begin{bmatrix} D_{xn} \\ D_{zn} \\ D_{\theta n} \end{bmatrix}_{3\times 1} \tag{8}$$

## 2.2 Modal absorbed energy of two-way asymmetric-plan buildings

Chopra and Goel (2004) pointed out that any response history, $r(t)$, of an asymmetric-plan system can be approximately estimated as

$$r(t) \approx \sum_{n=1}^{3N} r_n(t) \tag{9}$$

where $r_n(t)$ is the $n$-th modal response history. The accuracy of the assumption of uncoupled modal responses for inelastic structures, i.e. Eq. 9, were validated by investigating the displacements and storey drifts of three 9-storey asymmetric-plan steel buildings (Chopra and Goel 2004). The maximum values of the storey drifts of the stated three steel buildings were larger than 3%. According to the provisions of FEMA (2000), these example buildings were severely damaged and in a state between the performance levels of life safety and collapse prevention. Hence, the assumption of uncoupled "modal" responses (Eq. 9) should be applicable to most of the common structural evaluations. Prasanth et al. (2008) indeed confirmed the application of the approximation shown in Eq. 9 to the estimation of the energy demands of symmetric-plan buildings. In this study, Eq. 9 is applied to estimate the absorbed energy of asymmetric-plan buildings by using the 3DOF modal systems. The proposed approach is stated as follows:

Both sides of Eq. 3 multiplied by the increment of the $n$-th modal displacement response, $\Delta\mathbf{u}_n$, yields

$$\Delta E_{kn} + \Delta E_{\xi n} + \Delta E_{an} = \Delta E_{in} \tag{10}$$

where the incremental kinetic energy $\Delta E_{kn}$, incremental damping energy $\Delta E_{\xi n}$, incremental absorbed energy $\Delta E_{an}$, and the incremental input energy, $\Delta E_{in}$, can be expressed as

$$\begin{aligned} &\Delta E_{kn} = (\mathbf{M}\ddot{\mathbf{u}}_n)^T \Delta\mathbf{u}_n,\ \Delta E_{\xi n} = (\mathbf{C}\dot{\mathbf{u}}_n)^T \Delta\mathbf{u}_n,\ \Delta E_{an} = \mathbf{R}^T\Delta\mathbf{u}_n = \left(\hat{\mathbf{K}}\mathbf{u}_n\right)^T \Delta\mathbf{u}_n, \\ &\Delta E_{in} = -\left(\Gamma_{xn}\ddot{u}_{gx} + \Gamma_{zn}\ddot{u}_{gz}\right)\left(\mathbf{M}\boldsymbol{\varphi}_n\right)^T \Delta\mathbf{u}_n \end{aligned} \tag{11}$$

$\mathbf{R}$ is the restoring force vector of the original building, which is equal to the secant stiffness, $\hat{\mathbf{K}}$, multiplied by the modal displacement response, $\mathbf{u}_n$. The restoring force of the $n$-th 3DOF modal system, denoted as $[V_{xn} \quad V_{zn} \quad T_n]^T$, is

$$\left[V_{xn} \quad V_{zn} \quad T_n\right]^T = \hat{\mathbf{K}}_n\mathbf{D}_n = \mathbf{\Phi}_n^T\hat{\mathbf{K}}\mathbf{\Phi}_n\mathbf{D}_n \tag{12}$$

where $\hat{\mathbf{K}}_n$ is the $3 \times 3$ secant stiffness of the $n$-th 3DOF modal system. Using Eqs. 8, 9, 11 and 12, the total absorbed energy $E_a$ of a two-way asymmetric-plan building subjected to bi-directional ground motions is

$$\begin{aligned} E_a(t) &\approx \sum_{n=1}^{3N} E_{an}(t) = \sum_{n=1}^{3N} \int_0^t \Delta E_{an} = \sum_{n=1}^{3N} \int_0^t \mathbf{R}^T \Delta \mathbf{u}_n = \sum_{n=1}^{3N} \int_0^t \left(\hat{\mathbf{K}}\mathbf{u}_n\right)^T \Delta \mathbf{u}_n \\ &= \sum_{n=1}^{3N} \int_0^t \left(\hat{\mathbf{K}}\boldsymbol{\Phi}_n\mathbf{D}_n\right)^T \boldsymbol{\Phi}_n \Delta \mathbf{D}_n = \sum_{n=1}^{3N} \int_0^t \left(\hat{\mathbf{K}}_n\mathbf{D}_n\right)^T \Delta \mathbf{D}_n = \sum_{n=1}^{3N} \int_0^t \begin{bmatrix} V_{xn} & V_{zn} & T_n \end{bmatrix} \Delta \mathbf{D}_n \\ &= \sum_{n=1}^{3N} \left( \int_0^t V_{xn} \Delta D_{xn} + \int_0^t V_{zn} \Delta D_{zn} + \int_0^t T_n \Delta D_{\theta n} \right) \\ &= \sum_{n=1}^{3N} E_{an}^{xx}(t) + \sum_{n=1}^{3N} E_{an}^{zz}(t) + \sum_{n=1}^{3N} E_{an}^{\theta\theta}(t) = E_{ax}(t) + E_{az}(t) + E_{a\theta}(t) \end{aligned} \tag{13}$$

where $E_{an}^{xx}(t)$, $E_{an}^{zz}(t)$ and $E_{an}^{\theta\theta}(t)$ are

$$E_{an}^{xx}(t) = \int_0^t V_{xn} \Delta D_{xn}, \quad E_{an}^{zz}(t) = \int_0^t V_{zn} \Delta D_{zn}, \quad E_{an}^{\theta\theta}(t) = \int_0^t T_n \Delta D_{\theta n} \tag{14}$$

$E_a(t)$ is the cumulative absorbed energy up to time $t$. Furthermore, Eq. 13 indicates that the $n$-th modal absorbed energy $E_{an}$ of a two-way asymmetric-plan building is the summation of $E_{an}^{xx}$, $E_{an}^{zz}$ and $E_{an}^{\theta\theta}$, which represent the modal absorbed energies contributed from the X-, Z-translational and Y-rotational deformations, respectively. Therefore, the total absorbed energy $E_a$ consists of three portions, i.e. $E_{ax}$, $E_{az}$ and $E_{a\theta}$, representing the absorbed energies resulting from the three different types of deformation. In this study, the modal absorbed energy $E_{an}$ is obtained by using the step-by-step integration of the 3DOF modal equation of motion (Eq. 4). Since the higher modes of structures usually remain elastic under earthquake loads (Chopra et al. 2004), only the first few vibration modes need to be considered for computing the absorbed energy. Therefore, the proposed method is more efficient than the computation-intensive nonlinear RHA method applied to the whole building system. Furthermore, by using the proposed method, the absorbed energies contributed from different types of structural deformation are available, which seems never explored before.

### 2.3 The relationships between the signs of modal eccentricities and the trend of plan-wise distribution of modal absorbed energy

By comparing the structural properties of asymmetric-plan buildings with those of the corresponding uncoupled buildings, it is evident that the global eccentricity, the distance between the center of mass (CM) and the center of rigidity (CR), is the only structural parameter causing the uneven distribution of absorbed energy on the floor-plan edges of asymmetric-plan building. Nevertheless, from past researches, it has been demonstrated that the global eccentricity is an inappropriate index for reasoning the trend of plan-wise distribution of absorbed energy of asymmetric-plan buildings. Besides the global eccentricity, the characteristics of ground motions are also the factors affecting the mentioned distribution. In this study, the modal eccentricities, $e_{xn}$ and $e_{zn}$, instead of global eccentricity are investigated. The characteristics of ground motions are not in the scope of this study.

**Table 1** The relationships between the signs of modal eccentricities and the floor-plan edge with large modal absorbed energy demand among the two edges in each horizontal direction.

| Combination | | The floor-plan edges with large energy demand | |
|---|---|---|---|
| Sign($e_{xn}$) | Sign($e_{zn}$) | Z-dir. | X-dir. |
| + | + | SS | FS |
| + | − | SS | SS |
| − | + | FS | FS |
| − | − | FS | SS |

The FS and SS of an asymmetric-plan building are defined as the floor-plan edges close to CM and CR respectively (Fig. 1b). The sign conventions of modal eccentricities and global eccentricities $e_x$ and $e_z$ are shown in Fig. 1a, b, respectively. By comparing Fig. 1a with Fig. 1b, the FS of a 3DOF modal system is the end of the rigid beam with lumped mass. The other end of the rigid beam connected to the top of the column is the SS of a 3DOF modal system. While a positive rotation of the rigid beam of a 3DOF modal system occurs, the 3DOF modal system with positive $e_{zn}$ ($e_{xn}$) has a positive (negative) increment of X (Z)-translation on the FS (Fig. 1a). Thus, the absorbed energy increases (decreases) on the FS in the X (Z)-direction of the 3DOF modal system due to the positive rotation of the rigid beam. At the same time, the absorbed energy decreases (increases) on the SS in the X (Z)-direction. Thus, the trend of the plan-wise distribution of modal absorbed energy for asymmetric-plan buildings can be anticipated by using the signs of the modal eccentricities. For example, the modal absorbed energy of the $n$-th vibration mode with positive $e_{xn}$ and $e_{zn}$ will much concentrate on the SS and FS in the Z- and X-directions, respectively. The signs of modal eccentricities are symbolized by sign($e_{xn}$) and sign($e_{zn}$) in the rest of this paper. Considering all possible combinations of sign($e_{xn}$) and sign($e_{zn}$), Table 1 shows the relationships between the signs of modal eccentricities and the floor-plan edge with large modal absorbed energy demand among the two edges in each horizontal direction.

The trend of the plan-wise distribution of total absorbed energy is an integral result from all modal absorbed energies. Furthermore, the amount of each modal absorbed energy is dependent upon the characteristics of ground motions. Therefore, the trend of the plan-wise distribution of total absorbed energy of asymmetric-plan buildings not only is affected by the modal eccentricities but also may be changed from earthquake to earthquake. That is why the diverse conclusions about the uneven distribution of total absorbed energy of asymmetric-plan buildings were observed from the global eccentricities.

## 3 Numerical validation

The objectives of this section are to validate the efficiency of the proposed method and the correctness of the relationships between the signs of modal eccentricities and the trend of the uneven distribution of modal absorbed energy on floor-plan edges of asymmetric-plan buildings.

### 3.1 The selected structural system, ground motions and basic assumptions

The example buildings are one 3-storey and one 20-storey two-way asymmetric-plan buildings with the perimeter moment frames shown in Fig. 2. Each floor is simulated as a rigid diaphragm. The CR is at the geometric center of the floor plan. The 3-storey building is

2@5 m long, 2@5 m wide and 3@3.5 m tall. The 20-storey building is a variation of the 20-storey symmetric-plan building used in the SAC Steel Research Project for the investigation of buildings located in Los Angeles (Krawinkler 2000). This stated variation is the CM of the 20-storey symmetric-plan building moved away from the CR with the eccentricity ratios equal to 20% in both X- and Z-directions. The materials of the beams and columns used in the 20-storey building are Dual A36 Gr. 50 steel and A572 Gr. 50 steel, respectively. The yield strength of these two steel types used in the analysis is 340 and 345 MPa, respectively. The details of the member sizes and mass distribution of the 20-storey building can be found in the original report (Krawinkler 2000). The CM of the 3-storey building is eccentrically located with eccentricity ratios equal to 25% in both X- and Z-directions. The steel material of the 3-storey building is A36 steel, which is simulated as a bilinear material with a yielding stress equal to 245 MPa, Young's modulus $E = 2.0 \times 10^5$ MPa and 5% post-yielding stiffness ratio. The member sizes of the columns and beams of the 3-storey building are H200 × 200 × 12 × 12 and H200 × 150 × 6 × 9, respectively. The mass and the mass moment of inertia for each floor of the 3-storey building are respectively equal to 50,000 kg and $8.33 \times 10^5$ kg-m$^2$. Rayleigh damping with 5% damping ratios for the first two vibration modes of these two example buildings are assumed. The modal properties of the two example buildings are shown in Table 2. Table 2 indicates that, up to the fifth vibration mode of the two example buildings, the accumulative modal participation mass ratios are greater than 90% of the total mass in both horizontal directions. Recall that the hysteretic energy demand of the SAC 20-storey building has been investigated by Prasanth et al. (2008) using the modal pushover analysis. That research pointed out that only the first three vibration modes of the SAC 20-storey building were needed to compute the hysteretic energy demand because the 4th and 5th vibration modes were found to be elastic under the excitation of a total of 18 ground motion records. Furthermore, the 3rd vibration mode would become inelastic only when certain four of the 18 ground motions are exerted. Thus, in this study, only the first five vibration modes of the two example buildings are considered for estimating the total absorbed energy.

In order to validate the proposed method, the example buildings are subjected to maximum credible earthquakes (MCEs) as considered in the SAC Steel Research Project (Krawinkler 2000). Under the MCE excitations with a return period of 2,475 years (2% chance of exceedance in 50 years), the example buildings are likely severely damaged. In this manner, the absorbed energy demands can be investigated. The applied direction of each component of the bi-directional ground motions is also shown in Table 3a. The pseudo-acceleration (PSA) response spectra of these selected ground motions are illustrated in Fig. 3a. Except the 2nd loading case (Table 3a), i.e. LA23 and LA24, the ordinates of the PSA response spectra are very small in the range of long vibration periods (Fig. 3a). Thus, since the periods of the first two vibration modes of the 20-storey example building are 4.11 and 3.57 s (Table 2b), only LA23 and LA24 ground motions are selected for the history analysis of the 20-storey example building. In addition to LA23 and LA24 ground motions, LA03 and LA04 ground motions with 475 years return period in the SAC steel research project are amplified 1.5 times for the history analysis of the 20-storey example building. Thus, there are a total of two loading cases for this 20-storey example building (Table 3b). The PSA response spectra of these selected ground motions for the 20-storey example building are shown in Fig. 3b. The tools for the structural analyses and the visualization of the analytical results are the PISA3D and GISA3D computer programs (Lin et al. 2009), respectively.

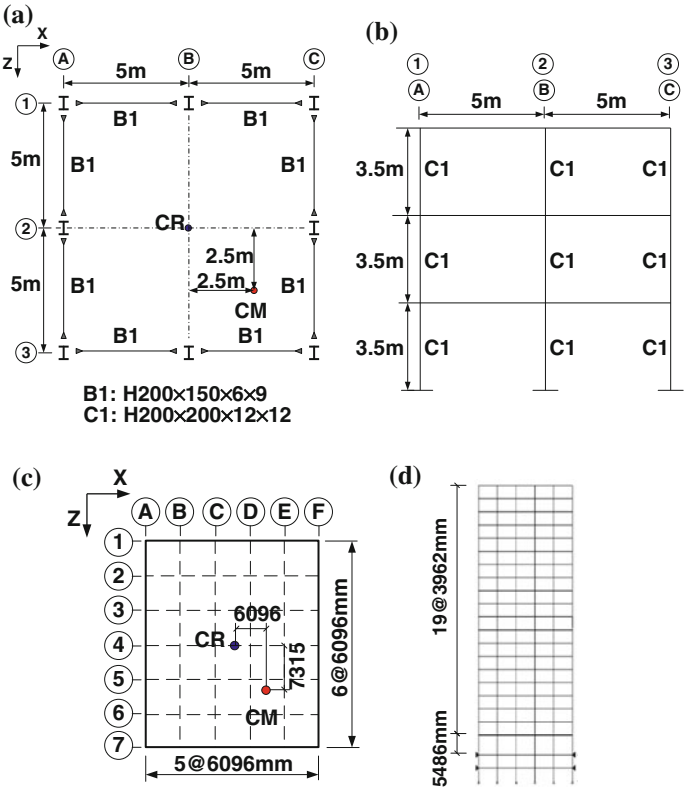


**Fig. 2** **a** The typical floor plan and **b** the elevation of the 3-storey example building **c** The typical floor plan and **d** the elevation of the 20-storey example building

### 3.2 Discussion of analytical results

By using Eqs. 6 and 7, the 3DOF modal properties for the first five vibration modes of the 3-storey and 20-storey example buildings are obtained as shown in Table 4a–d. The force-deformation relationships of the first five vibration modes of the example buildings are illustrated in Fig. 4. The thin lines and thick lines shown in Fig. 4 are the force-deformation curves respectively obtained from the pushover analyses of the example buildings and the associated 3DOF modal systems. In this study, the units of the mode shape, $\boldsymbol{\varphi}_{xn}$, $\boldsymbol{\varphi}_{zn}$ and $\boldsymbol{\varphi}_{\theta n}$ of the 20-storey example building adopt mm, mm and radian, respectively. Thus, the modal response values, $D_{xn} = u_{xn,r}/\boldsymbol{\varphi}_{xn,r}$, $D_{zn} = u_{zn,r}/\boldsymbol{\varphi}_{zn,r} D_{\theta n} = u_{\theta n,r}/\boldsymbol{\varphi}_{\theta n,r}$ (Lin and Tsai 2008), presented in the x-axis of Fig. 4 are dimensionless. Therefore, since the unit of the mode shape of the 20-story example building is rather small, the response values shown in the abscissa of Fig. 4b are possible. Fig. 4 shows that the three force-deformation curves of each vibration mode of the example buildings are simultaneously and satisfactorily simulated by using the corresponding 3DOF modal system. According to the signs of modal eccentricities (Table 4a, c), the floor-plan edge of the example buildings with large modal absorbed energy demand among the two edges in each horizontal direction is predicted as shown in Table 4e, f. Figure 5a, b respectively show the distributions of the positive and negative accumulative plastic hinge rotations of the 3-storey and the 20-storey example buildings at the end

**Table 2** Modal properties of the example buildings

| Mode no. | 1 | 2 | 3 | 4 | 5 | 6 | 7 | 8 | 9 |
|---|---|---|---|---|---|---|---|---|---|
| *(a) The 3-storey example building* | | | | | | | | | |
| Vibration period (s) | 1.93 | 1.49 | 0.78 | 0.59 | 0.43 | 0.33 | 0.23 | 0.22 | 0.12 |
| Dominant motion | X | Z | R | X | Z | X | Z | R | X |
| Modal participation mass ratio (%) | | | | | | | | | |
| X-tran. | 76 | 8 | 2 | 10 | 1 | 3 | 0 | 0 | 0 |
| Z-tran. | 6 | 70 | 6 | 1 | 12 | 0 | 0 | 4 | 1 |
| Y-rot. | 4 | 4 | 76 | 0 | 0 | 0 | 11 | 0 | 3 |
| Accumulative modal participation mass ratio (%) | | | | | | | | | |
| X-tran. | 76 | 84 | 86 | 96 | 97 | 100 | 100 | 100 | 100 |
| Z-tran. | 6 | 76 | 82 | 83 | 95 | 95 | 95 | 99 | 100 |
| Y-rot. | 4 | 8 | 85 | 85 | 86 | 86 | 97 | 97 | 100 |
| *(b) The 20-storey example building* | | | | | | | | | |
| Vibration period (s) | 4.11 | 3.57 | 1.87 | 1.45 | 1.26 | 0.86 | 0.75 | 0.66 | 0.61 |
| Dominant motion | X | Z | R | X | Z | X | R | Z | R |
| Modal participation mass ratio (%) | | | | | | | | | |
| X-tran. | 68 | 10 | 2 | 9 | 1 | 3 | 1 | 0 | 2 |
| Z-tran. | 9 | 69 | 2 | 1 | 9 | 0 | 3 | 0 | 0 |
| Y-rot. | 4 | 1 | 77 | 0 | 0 | 0 | 0 | 9 | 0 |
| Accumulative modal participation mass ratio (%) | | | | | | | | | |
| X-tran. | 68 | 78 | 80 | 89 | 90 | 93 | 94 | 94 | 96 |
| Z-tran. | 9 | 78 | 80 | 82 | 90 | 91 | 94 | 94 | 94 |
| Y-rot. | 4 | 5 | 82 | 82 | 82 | 82 | 82 | 91 | 91 |

of the pushover analyses. In order to obviously tell the difference between the distribution of the plastic hinge rotations on FS and that on SS of the 20-storey building under the 2nd modal pushover analysis, the perspective view shown in Fig. 5b is further two-dimensionally illustrated in Fig. 5c. Figure 5 shows that the floor-plan edge with large modal absorbed energy demand among the two edges in each horizontal direction is the same as that predicted in Table 4e, f. Therefore, the relationships between the signs of modal eccentricities and the trend of the uneven distribution of the modal absorbed energy on floor-plan edges are confirmed.

The total absorbed energy estimated by using the proposed method and the nonlinear RHA method for the whole building are respectively denoted as $E_{a,3DOF}$ and $E_{a,RHA}$. $E_{a,RHA}$ is regarded as the benchmark solution in this study. Furthermore, the absorbed energy of the corresponding symmetric-plan building is also computed by using the nonlinear RHA method and denoted as $E_{a,RHA0}$. The values of $E_{a,3DOF}$, $E_{a,RHA}$ and $E_{a,RHA0}$ of the two example buildings under the exertion of all loading cases are listed in Table 5. Table 5 indicates that the total absorbed energy demands of the two example buildings are satisfactorily estimated by using the proposed method. Furthermore, the value of $E_{a,RHA}/E_{a,RHA0}$ varied from 0.96 to 1.47 (Table 5) indicates that the total absorbed energy of an asymmetric-plan building is not always greater than that of the corresponding symmetric-plan building. However, due to the unevenly plan-wise distribution of the absorbed energy, asymmetric-plan buildings may still be more vulnerable to earthquakes than the corresponding symmetric-plan buildings.

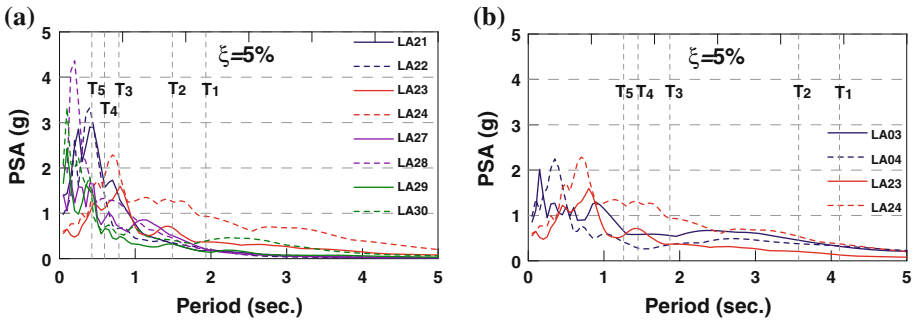


**Fig. 3** The pseudo-acceleration response spectra with 5% damping ratio for the selected ground motion records for **a** the 3-storey example building and **b** the 20-storey example building

**Table 3** Earthquake data

| Loading case | Designation | Record information | Duration (s) | Magnitude $M_w$ | $R$ (km) | Scale | PGA (g) | Applied direction |
|---|---|---|---|---|---|---|---|---|
| (a) The 3-storey example building | | | | | | | | |
| 1 | LA21 | 1995 Kobe | 59.98 | 6.9 | 3.4 | 1.15 | 1.28 | X |
| | LA22 | 1995 Kobe | 59.98 | 6.9 | 3.4 | 1.15 | 0.92 | Z |
| 2 | LA23 | 1989 Loma Prieta | 24.99 | 7.0 | 3.5 | 0.82 | 0.42 | X |
| | LA24 | 1989 Loma Prieta | 24.99 | 7.0 | 3.5 | 0.82 | 0.47 | Z |
| 3 | LA27 | 1994 Northridge | 59.98 | 6.7 | 6.4 | 1.61 | 0.93 | X |
| | LA28 | 1994 Northridge | 59.98 | 6.7 | 6.4 | 1.61 | 1.33 | Z |
| 4 | LA29 | 1974 Tabas | 49.98 | 7.4 | 1.2 | 1.08 | 0.81 | X |
| | LA30 | 1974 Tabas | 49.98 | 7.4 | 1.2 | 1.08 | 0.99 | Z |
| (b) The 20-storey example building | | | | | | | | |
| 1 | LA03 | 1979 Imperial Valley | 39.38 | 6.5 | 4.1 | 1.52 | 0.59 | X |
| | LA04 | 1979 Imperial Valley | 39.38 | 6.5 | 4.1 | 1.52 | 0.73 | Z |
| 2 | LA23 | 1989 Loma Prieta | 24.99 | 7.0 | 3.5 | 0.82 | 0.42 | X |
| | LA24 | 1989 Loma Prieta | 24.99 | 7.0 | 3.5 | 0.82 | 0.47 | Z |

The ratios of the modal absorbed energy, $E_{an}$, to the total absorbed energy, $E_{a,3DOF}$, are illustrated in Fig. 6. The distributions of the positive and negative accumulative plastic hinge rotations of the example buildings under the exertion of the selected ground motions are illustrated in Fig. 7. Figure 6a shows that the 3rd vibration mode of the 3-storey example building is elastic under the exertion of all the selected ground motions. The 4th and the 5th vibration modes of the 3-storey example building have obvious contribution to the total absorbed energy only at the first loading case. Figure 6a also shows that the 2nd vibration mode is overwhelmingly dominant for the total absorbed energy of the 3-storey example building under the exertion of the 2nd and the 3rd loading cases. Thus, by using the signs of modal eccentricities (Table 4e), it can be anticipated that the total absorbed energy of the 3-storey example building under the 2nd and the 3rd loading cases will be obviously concentrated on the FS and SS in the Z- and X-directions, respectively. The actual distributions of the accumulative plastic hinge rotations at the end of the nonlinear RHA of the two example buildings are shown in Fig. 7. From Fig. 7a, it confirms the mentioned anticipation that the

**Table 4** The 3DOF modal properties of the example buildings

| Mode | $m_{xn}$ | $m_{zn}$ | $I_n$ | $k_{xn}$ | $k_{zn}$ | $k_{\theta n}$ | $e_{xn}$ | $e_{zn}$ | $\beta_n$ |
|---|---|---|---|---|---|---|---|---|---|
| (a) The elastic 3DOF modal properties of the 3-storey example building | | | | | | | | | |
| 1 | 0.882 | 0.070 | 0.046 | 10.848 | 1.473 | 2.156 | −0.497 | 0.139 | 2.26E-04 |
| 2 | 0.097 | 0.852 | 0.052 | 1.199 | 17.815 | 2.436 | −0.151 | −0.445 | −2.19E-03 |
| 3 | 0.019 | 0.080 | 0.902 | 0.244 | 1.889 | 44.261 | 1.713 | −3.993 | −6.85E-06 |
| 4 | 0.920 | 0.042 | 0.038 | 117.530 | 11.234 | 19.732 | −0.583 | 0.124 | 4.90E-06 |
| 5 | 0.065 | 0.850 | 0.084 | 8.334 | 227.580 | 43.745 | −0.191 | −0.692 | 2.42E-06 |
| Mode | $k'_{xn}$ | $k'_{zn}$ | $k'_{\theta n}$ | $M_{yxn}$ | $M_{yzn}$ | $M_{y\theta n}$ | | | |
| (**b**) The inelastic 3DOF modal properties of the 3-storey example building | | | | | | | | | |
| 1 | 3.479 | 1.498 | 0.933 | 9.701 | 0.772 | 2.241 | | | |
| 2 | 0.629 | 7.257 | 0.555 | 1.851 | 16.184 | 2.608 | | | |
| 3 | 0.054 | 0.481 | 13.367 | 0.604 | 2.547 | 22.013 | | | |
| 4 | 39.750 | 10.657 | 7.827 | 22.087 | 1.005 | 4.231 | | | |
| 5 | 1.595 | 57.424 | 7.830 | 3.912 | 51.010 | 12.120 | | | |
| Mode | $m_{xn}$ | $m_{zn}$ | $I_n$ | $k_{xn}$ | $k_{zn}$ | $k_{\theta n}$ | $e_{xn}$ | $e_{zn}$ | $\beta_n$ |
| (c) The elastic 3DOF modal properties of the 20-storey example building | | | | | | | | | |
| 1 | 0.848 | 0.108 | 0.044 | 2.262 | 0.355 | 0.418 | −0.283 | 0.122 | −4.80E-04 |
| 2 | 0.127 | 0.861 | 0.012 | 0.341 | 2.817 | 0.112 | −0.052 | −0.161 | −5.76E-03 |
| 3 | 0.027 | 0.031 | 0.941 | 0.093 | 0.111 | 9.233 | 2.154 | −2.220 | 1.44E-03 |
| 4 | 0.839 | 0.114 | 0.047 | 18.079 | 2.989 | 3.467 | −0.281 | 0.124 | −9.94E-05 |
| 5 | 0.134 | 0.855 | 0.012 | 2.887 | 22.449 | 0.866 | −0.052 | −0.156 | −7.18E-04 |
| Mode | $k'_{xn}$ | $k'_{zn}$ | $k'_{\theta n}$ | $M_{yxn}$ | $M_{yzn}$ | $M_{y\theta n}$ | | | |
| (d) The inelastic 3DOF modal properties of the 20-storey example building | | | | | | | | | |
| 1 | 0.969 | 0.340 | 0.137 | 2289.600 | 291.600 | 480.650 | | | |
| 2 | 0.303 | 0.660 | 0.027 | 508.000 | 3444.000 | 144.450 | | | |
| 3 | 0.034 | 0.064 | 5.477 | 170.240 | 198.400 | 5217.100 | | | |
| 4 | 10.557 | 2.854 | 1.929 | 5797.500 | 787.740 | 1265.000 | | | |
| 5 | 2.489 | 10.567 | 0.205 | 1340.000 | 8550.000 | 351.590 | | | |

| Mode | Combination | | Sides with larger energy demand | |
|---|---|---|---|---|
| | Sign($e_{xn}$) | Sign($e_{zn}$) | Z-dir. | X-dir. |
| (e) The floor-plan edges of the 3-storey building with larger modal absorbed energy demand | | | | |
| 1 | − | + | FS | FS |
| 2 | − | − | FS | SS |
| 3 | + | − | SS | SS |
| 4 | − | + | FS | FS |
| 5 | − | − | FS | SS |

**Table 4** continued

| Mode | Combination | | Sides with larger energy demand | |
|---|---|---|---|---|
| | Sign($e_{xn}$) | Sign($e_{zn}$) | Z-dir. | X-dir. |
| (f) The floor-plan edges of the 20-storey building with larger modal absorbed energy demand | | | | |
| 1 | − | + | FS | FS |
| 2 | − | − | FS | SS |
| 3 | + | − | SS | SS |
| 4 | − | + | FS | FS |
| 5 | − | − | FS | SS |

**Table 5** The values of $E_{a,3DOF}$, $E_{a,RHA}$, and $E_{a,RHA0}$ for the example buildings

| Buildings | 3-storey example building | | | | 20-storey example building | |
|---|---|---|---|---|---|---|
| Loading case | 1 | 2 | 3 | 4 | 1 | 2 |
| $E_{a,3DOF}$ (kN-m) | 95.1 | 490.6 | 71.7 | 79.8 | 28886 | 22052 |
| $E_{a,RHA}$ (kN-m) | 102.4 | 566.9 | 94.8 | 100.8 | 30880 | 26810 |
| $E_{a,RHA0}$ (kN-m) | 79.2 | 593.6 | 97.3 | 68.54 | 30230 | 26810 |
| $E_{a,3DOF}/E_{a,RHA}$ | 0.93 | 0.87 | 0.76 | 0.79 | 0.94 | 0.82 |
| $E_{a,RHA}/E_{a,RHA0}$ | 1.29 | 0.96 | 0.97 | 1.47 | 1.02 | 1.00 |

total absorbed energy of the 3-storey building under the 2nd and the 3rd loading cases are obviously concentrated on the FS and SS in the Z- and X-directions, respectively. Figure 6a shows that the 1st and the 2nd vibration modes about equally contribute to the total absorbed energy of the 3-storey building under the 4th loading case. It is noted that the dominant types of motion for the 1st and the 2nd vibration modes of the 3-storey building are X- and Z-translation, respectively (Table 2a). Thus, by using the signs of modal eccentricities (Table 4e), it can be predicted that the total absorbed energy of the 3-storey example building under the 4th loading case will be much concentrated on the FS in both the X- and the Z-directions. Again, from the actual distributions of accumulative plastic hinge rotations shown in Fig. 7a, it confirms this prediction. Figure 6b shows that the 2nd vibration mode of the 20-storey example building is the dominant vibration mode for the selected two loading cases. Therefore, based on the signs of modal eccentricities shown in Table 4f, it can be predicted that the FS and SS of the 20-storey example building in the Z- and X-directions, respectively, are the floor-plan edges facing more energy demand, which are confirmed from Fig. 7b.

The portions of the modal absorbed energy contributed from different types of deformation, i.e. $E_{an}^{xx}$, $E_{an}^{zz}$, $E_{an}^{\theta\theta}$, are shown in Table 6. Table 6 shows that the dominant type of motion of each vibration mode (Table 2) has the largest portion of the modal absorbed energy. For example, the dominant type of motion for the 2nd vibration mode of the two example buildings is the Z-directional translation (Table 2), which takes the largest portion of the 2nd modal absorbed energy (Table 6). The ratios of the absorbed energy resulting from different types of deformation to the total absorbed energy of the two example buildings are also shown in Table 6. From the ratios shown in Table 6, it is found that the absorbed energy resulting from the rotational deformation of the 3-storey example building takes 22–30% of the total

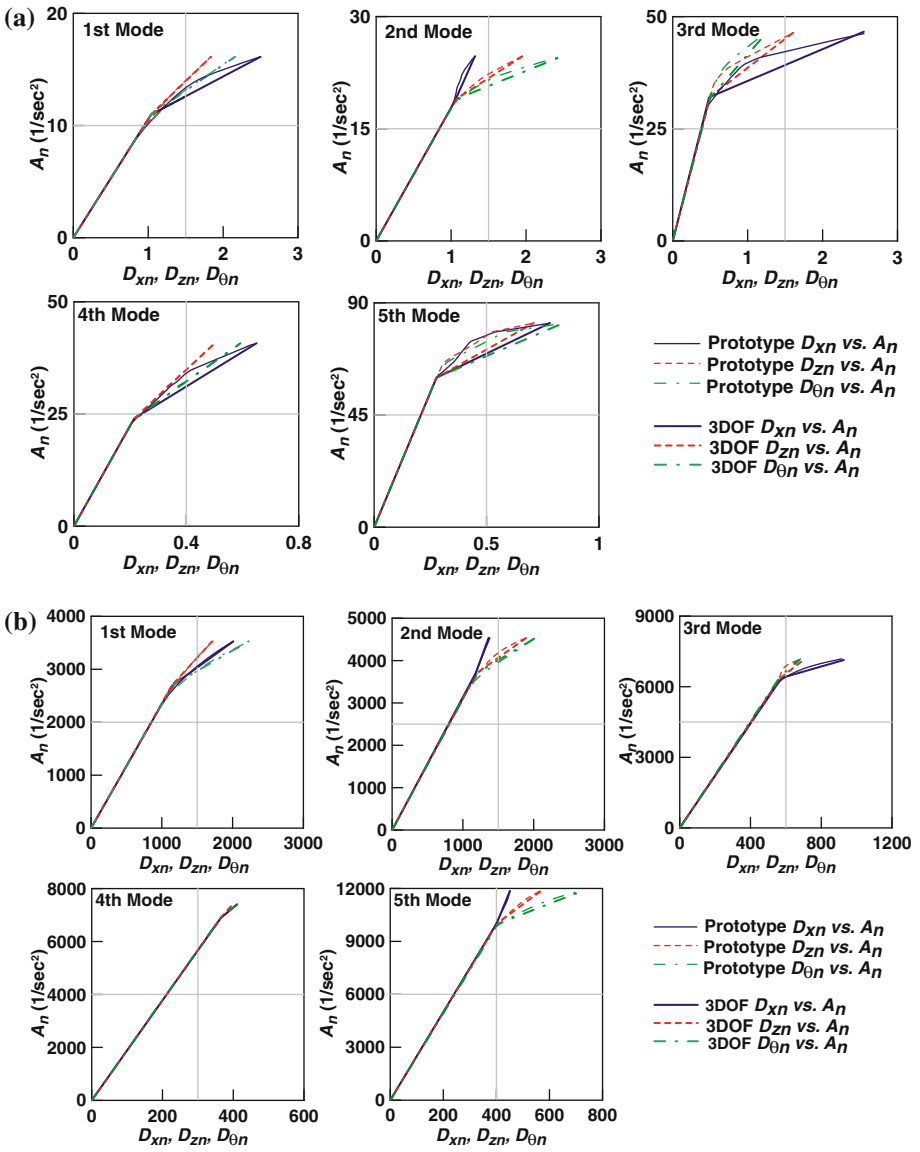


**Fig. 4** The modal force-deformation relationships of the first five vibration modes for **a** the 3-storey example building and **b** the 20-storey example building

absorbed energy. Nevertheless, the rotational deformation of the 20-storey example building has very little contribution to its total absorbed energy. That is to say, the accumulative damages of the 20-storey building under the exertion of the selected ground motions are caused by its translational deformation in the two horizontal directions. It implies that the strategies of the retrofit for these two example buildings should be different. For example, the retrofit of the 3-storey and the 20-storey example buildings should be respectively emphasized on the improvement of the rotational and translational energy dissipation capacities.

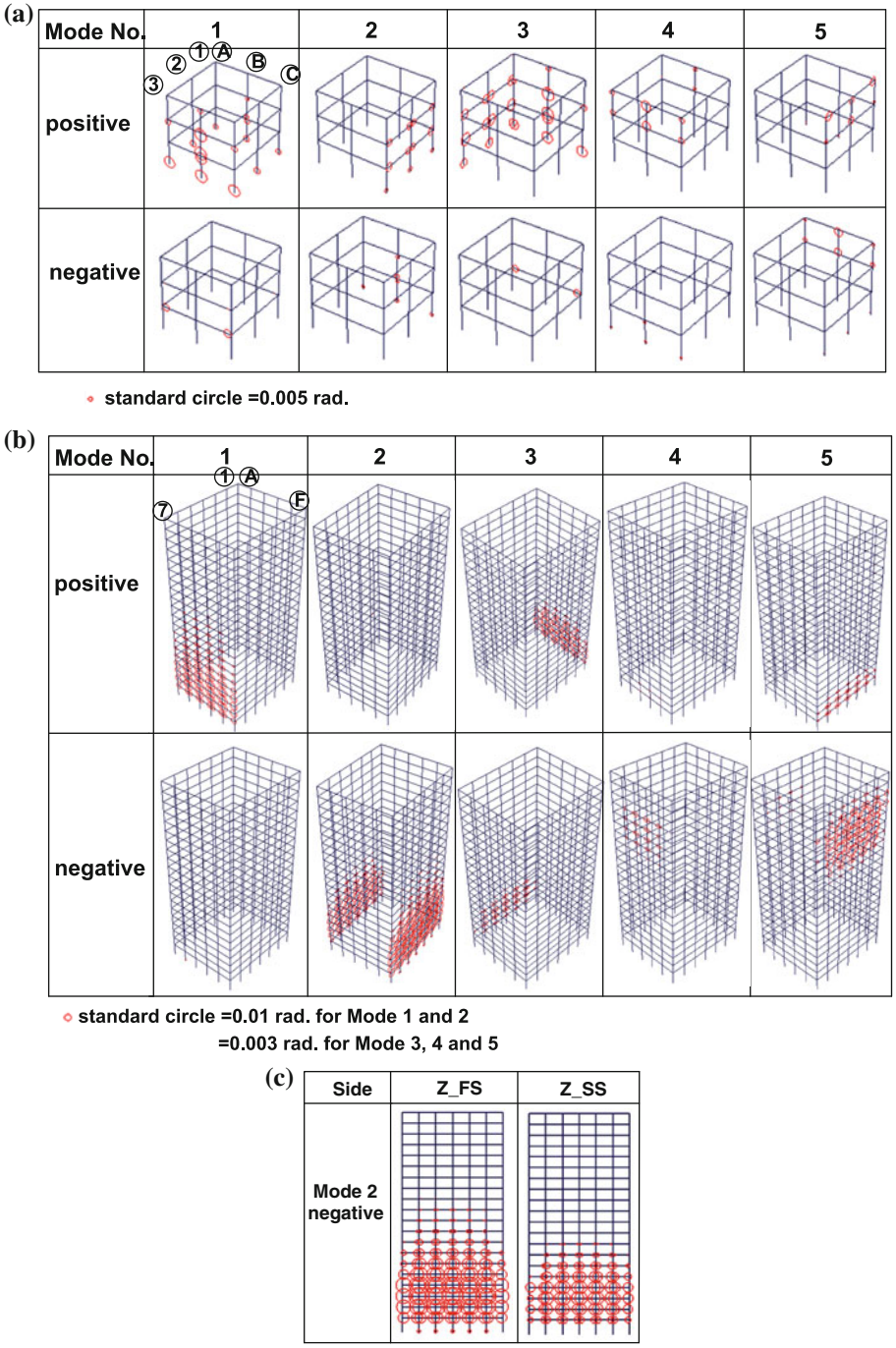


**Fig. 5** The distribution of the accumulative plastic hinge rotations of **a** the 3-storey example building **b** the 20-storey example building subjected to the first five modal inertia forces and **c** the two Z-directional frames of the 20-storey example building subjected to the 2nd modal inertia force

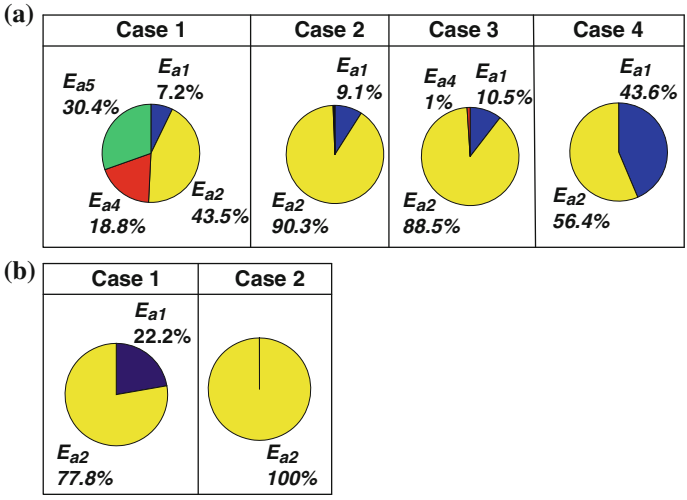


**Fig. 6** The ratios of the modal absorbed energy, $E_{an}$, to the total absorbed energy, $E_{a,3DOF}$, of **a** the 3-storey example building and **b** the 20-storey example building

As demonstrated in these examples, only the first few vibration modes need to be calculated for the estimation of the total absorbed energy. Thus, the proposed method is much efficient than performing the nonlinear RHA method for the whole multi-storey building. The analysis time required by using the laptop with 1.60 GHz central processing unit for the 20-storey example building is shown in Table 7. Table 7 indicates that the ratio of the analysis time of the proposed method to that of the nonlinear RHA method for the 20-storey building is only about 11%. Therefore, the computational efficiency of the proposed method is confirmed.

## 4 Summary and conclusions

Except the computation-intensive and time-consuming nonlinear RHA method, most of the available simplified methods for the estimation of seismic energy demand were developed for symmetric-plan buildings. This study provides an alternative approach to estimate the absorbed energy of two-way asymmetric-plan buildings subjected to bi-directional earthquake loads. The summary and conclusions of this study are as follows:

1. The total absorbed energy of two-way asymmetric-plan buildings can be satisfactorily estimated by using the 3DOF modal systems. The accuracy of the proposed method has been numerically validated by investigating one 3-storey and one 20-storey example buildings subjected to several bi-directional ground motions. The computational efficiency of the proposed method has been confirmed by comparing the analysis time required by using the proposed method with that required by using the nonlinear RHA method.
2. Instead of the global eccentricities, the modal eccentricities have been verified to be the accurate structural key parameters for reasoning the unevenly distributed absorbed energy of asymmetric-plan buildings. While the modal eccentricities, $e_{zn}$ and $e_{xn}$, are positive, the FS and SS in the X- and Z-directions, respectively, face larger modal absorbed energy demand than the other side of the floor plan in each direction. On the contrary, while

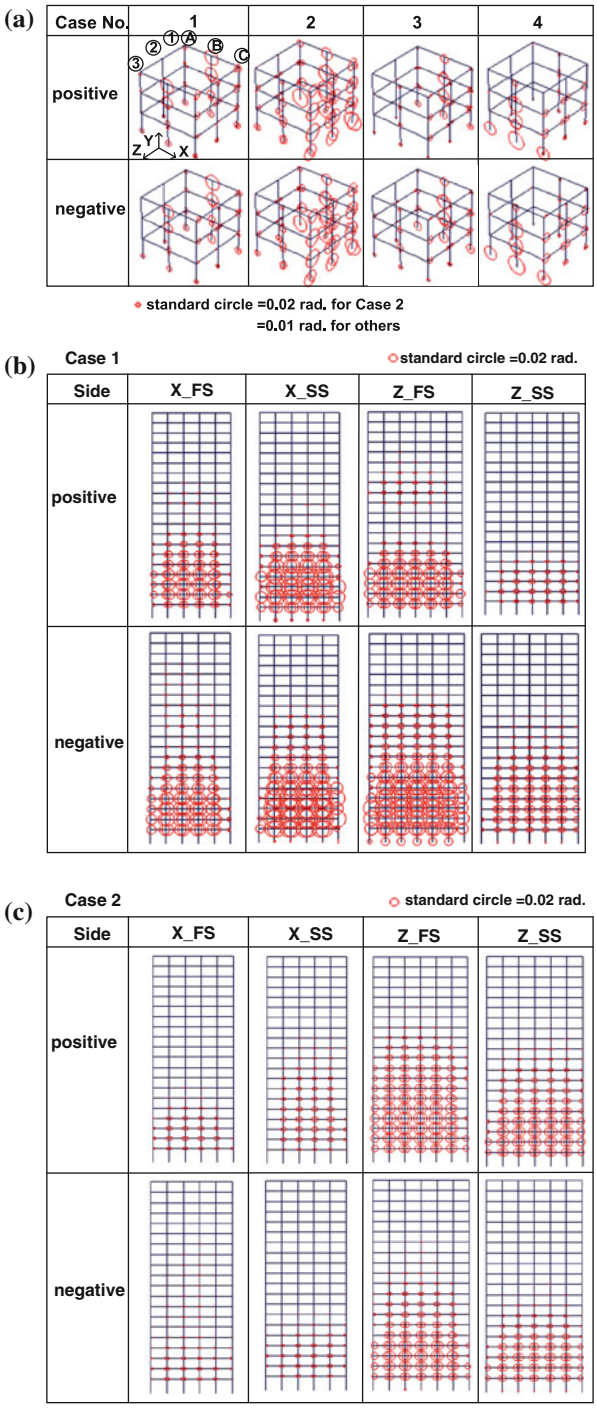


**Fig. 7** The distributions of the accumulative plastic hinge rotations for **a** the 3-storey example building subjected to the four loading cases, **b** the 20-storey example building subjected to the 1st loading case and **c** the 20-storey example building subjected to the 2nd loading case

**Table 6** The portions of modal absorbed energy contributed from different types of deformation (unit: kN-m)

| Mode no. | Case 1 | | | Case 2 | | | Case 3 | | | Case 4 | | |
|---|---|---|---|---|---|---|---|---|---|---|---|---|
| | $E_{an}^{xx}$ | $E_{an}^{zz}$ | $E_{an}^{\theta\theta}$ | $E_{an}^{xx}$ | $E_{an}^{zz}$ | $E_{an}^{\theta\theta}$ | $E_{an}^{xx}$ | $E_{an}^{zz}$ | $E_{an}^{\theta\theta}$ | $E_{an}^{xx}$ | $E_{an}^{zz}$ | $E_{an}^{\theta\theta}$ |
| (a) The 3-storey example building | | | | | | | | | | | | |
| 1 | 5.65 | −0.15 | 1.38 | 33.26 | −1.54 | 12.81 | 5.80 | −0.07 | 1.78 | 27.68 | −1.18 | 8.29 |
| 2 | 5.98 | 26.50 | 8.90 | 113.64 | 196.77 | 132.83 | 9.31 | 39.40 | 14.72 | 8.05 | 27.17 | 9.81 |
| 3 | 0.00 | 0.00 | 0.00 | −0.40 | −0.66 | 2.67 | 0.00 | 0.00 | 0.00 | 0.00 | 0.00 | 0.00 |
| 4 | 14.50 | −0.17 | 3.58 | 1.75 | 0.10 | −0.39 | 0.82 | 0.04 | −0.13 | 0.00 | 0.00 | 0.00 |
| 5 | 3.42 | 17.92 | 7.51 | 0.00 | 0.00 | 0.00 | 0.00 | 0.00 | 0.00 | 0.00 | 0.00 | 0.00 |
| Total | 29.56 | 44.11 | 21.37 | 148.25 | 194.67 | 147.92 | 15.94 | 39.38 | 16.36 | 35.73 | 26.00 | 18.10 |
| Ratio (%) | 31.1 | 46.4 | 22.5 | 30.2 | 39.7 | 30.1 | 22.2 | 54.9 | 22.8 | 44.8 | 32.6 | 22.7 |
| (b) The 20-storey example building | | | | | | | | | | | | |
| 1 | 5667 | 815 | −56 | 0 | 0 | 0 | | | | | | |
| 2 | 1286 | 21038 | 137 | 2658 | 19206 | 186 | | | | | | |
| 3 | 0 | 0 | 0 | 0 | 0 | 0 | | | | | | |
| 4 | 0 | 0 | 0 | 0 | 0 | 0 | | | | | | |
| 5 | 0 | 0 | 0 | −6 | 9 | −1 | | | | | | |
| Total | 6953 | 21853 | 80 | 2652 | 19215 | 185 | | | | | | |
| Ratio (%) | 24 | 76 | 0 | 12 | 87 | 1 | | | | | | |

**Table 7** The analysis time for the 20-storey example building

| Case no. | Analysis time using proposed method (s) | | | | | | Analysis time using nonlinear RHA (s) |
|---|---|---|---|---|---|---|---|
| | Mode 1 | Mode 2 | Mode 3 | Mode 4 | Mode 5 | Total | |
| 1 | 15.38 | 15.85 | 17.52 | 17.22 | 17.26 | 83.2 | 777.5 |
| 2 | 9.98 | 10.87 | 9.89 | 10.49 | 11.36 | 53.0 | 489.6. |

the modal eccentricities are negative, the modal absorbed energy is much concentrated on the SS and FS in the X- and Z-directions, respectively. The proposed relationship between the signs of modal eccentricities and the trend of uneven distribution of modal absorbed energy on the floor-plan edges has been verified by investigating the first five vibration modes of the two example buildings.

3. The portions of total absorbed energy contributed from different types of deformation can be respectively obtained by using the proposed method. This finding is new and academic interesting. Although this new finding may be useful for the decision of the retrofit policy for existing buildings, the concrete applications of this new finding to practical engineering is worthy of future research.

**Acknowledgments** The cooperation of B.Z. Lin and Y.J. Yu, the authors of PISA3D and M.C. Chuang, the author of GISA3D, in making the analytical tools available, is particularly appreciated.

## References

Chopra AK, Goel RK (2002) A modal pushover analysis procedure for estimating seismic demands for buildings. Earthq Eng Struct Dyn 31:561–582

Chopra AK, Goel RK (2004) A modal pushover analysis procedure to estimate seismic demands for unsymmetric-plan buildings. Earthq Eng Struct Dyn 33:903–927

Chopra AK, Goel RK, Chintanapakdee C (2004) Evaluation of a modified MPA procedure assuming higher modes as elastic to estimate seismic demands. Earthq Spectra 20(3):757–778

Chou CC (2001) An energy—based seismic evaluation procedure for moment resisting frame structures. Ph.D. Thesis, Department of Structural Engineering, University of California, San Diego, La Jolla, CA, USA

Chou CC, Uang CM (2003) A procedure for evaluating seismic energy demand of framed structures. Earthq Eng Struct Dyn 32:229–244

Fajfar P, Vidic T, Fischinger M (1989) Seismic demand in medium and long period structures. Earthq Eng Struct Dyn 18:1133–1144

FEMA-356 (2000) Prestandard and commentary for the seismic rehabilitation of buildings. Federal Emergency Management Agency, Washington, DC

Goel RK (1997) Seismic response of asymmetric systems: energy-based approach. J Struct Eng ASCE 123(11):1444–1453

Housner GW (1956) Limit design of structures to resist earthquake. In: Proceedings of 1st world conference on earthquake engineering, Berkeley, California, pp 5-1–5-13

Krawinkler H (2000) State of the art report on systems performance of steel moment frames subject to earthquake ground shaking. Report No. FEMA-355C SAC Joint Venture

Lin JL, Tsai KC (2008) Seismic analysis of two-way asymmetric building systems under bi-directional seismic ground motions. Earthq Eng Struct Dyn 37:305–328

Lin BZ, Chuang MC, Tsai KC (2009) Object-oriented development and application of a nonlinear structural analysis framework. Adv Eng Softw 40:66–82

Park YJ, Ang AHS (1985) Mechanistic seismic damage model for reinforced concrete. J Struct Eng ASCE 111(4):722–739

Prasanth T, Ghosh S, Collins KR (2008) Estimation of hysteretic energy demand using concepts of modal pushover analysis. Earthq Eng Struct Dyn 37:975–990